HHS Public Access

Author manuscript

Acta Biomater. Author manuscript; available in PMC 2020 January 15.

Published in final edited form as:

Acta Biomater. 2019 January 15; 84: 231–241. doi:10.1016/j.actbio.2018.11.005.

Freeze-Casting Porous Chitosan Ureteral Stents for Improved Drainage

Kaiyang Yin, **Prajan Divakar**, **Ulrike G.K. Wegst**

Thayer School of Engineering, Dartmouth College 14 Engineering Dr., Hanover, NH 03755, USA

Abstract

As a new strategy for improved urinary drainage in parallel to the potential for additional functions such as drug release and self-removal, highly porous chitosan stents are manufactured by radial, bi-directional freeze-casting. Inserting the porous stent in a silicone tube to emulate its placement in the ureter shows that it is shape conforming and remains safely positioned in place, also during flow tests, including those performed in a peristaltic pump. Cyclic compression tests on fully-hydrated porous stents reveal high stent resilience and close to full elastic recovery upon unloading. The drainage performance of the chitosan stent is evaluated, using effective viscosity in addition to volumetric flow and flux; the porous stent's performance is compared to that of the straight portion of a commercial 8 Fr double-J stent which possesses, in its otherwise solid tube wall, regularly spaced holes along its length. Both the porous and the 8 Fr stent show higher effective viscosities when tested in the silicone tube. The performance of the porous stent improves considerably more (47.5%) than that of the 8 Fr stent (30.6%) upon removal from the tube, illustrating the effectiveness of the radially aligned porosity for drainage. We conclude that the newly-developed porous chitosan ureteral stent merits further in vitro and in vivo assessment of its promise as an alternative and complement to currently available medical devices.

Keywords

bi-directional freezing; flow; flux; cyclic loading; radial structure

1. Introduction

The healthy ureter in an adult is a narrow, muscular tube of 24–30 cm in length and 2–4 mm in intraluminal diameter [1]. It carries the urine from the kidney to the bladder. Ureteral stents are tubes that are implanted in the ureter to drain urine from the kidney to the bladder. Typical indications fall into three categories: i) placement after surgical intervention performed as treatment of congenital obstructions, surgical reconstruction of the renal pelvis (pyeloplasty), the treatment of ureteral fistulae [2] or other ureteric repair with the goal to promote healing of the urothelium and ureteral wall, and, where required, also aiding the alignment of the ureteral walls, and decrease inflammation [3,4]; ii) placement after ureteric and kidney stone-related procedures (e.g. nephrolithotomy, nephrolithotripsy), or after endourological procedures, and iii) placement to maintain long-term patency of a ureter that

Tel: 1-603-646-3148, ulrike.wegst@dartmouth.edu.

is obstructed by a tumor [3,4]. Over 650,000 ureteral stent procedures are performed annually in the U.S., mostly utilizing traditional non-degradable, rigid polymeric or metallic ureteral stents [5].

The ideal ureteral stent, which is yet to be developed: i) can easily be inserted from any access point, ii) is resistant to migration, iii) possesses optimal flow characteristics, and iv) is non-refluxing, v) is biocompatible, vi) biodurable/biodegradable (depending on the indication), vii) resistant to encrustation, viii) radio-opaque/echodense (i.e. easily located using X-rays or ultrasound), ix) easily replaced, x) well tolerated by the patient (causing minimal pain and irritation), and xi) cost effective [3,4]. The typical polymeric ureteral stent currently in clinical use has a stiff and straight central stent region and ends in coils at either end to hold it in position in the ureters; these coils give rise to the name double-J stent [6].

Ureteral stents are available in a large range of lengths (18 – 32 cm) and diameters (typically 5 – 8 Fr, 1 Fr = 0.33 mm). Stent length selection depends primarily on the patient's height. This is because a patient's height is a more reliable indicator than a direct ureteric measurement, particularly, when the ureter is dilated and tortuous [7,8]. In children, a good predictor of required length is stent length = patient age in years + 10 [9].

Stent diameter selection is less rigorous, with larger diameters being favored over smaller ones, because they tend to migrate less distally and dislodge less often, while pain and irritative symptoms are not significantly affected by size. The stent's size is defined by the device's outer diameter. Frequently, stents in the range of 5 Fr to 8 Fr are used both in adults and children. The dimeter of the stent lumen typically varies from 1.0 mm to 2.0 mm. Interestingly, recent studies comparing stent sizes from 4.8–14 Fr show that, stent diameter does not correlate with stent-related voiding symptoms and pain. [10–12]

A hydrophilic surface of stents leads to the formation of a water film that enhances flow for given lumen and outer diameters [13]. To enhance drainage, and preserve drainage under the circumstances of stone and adjacent tumor, some stent designs include holes along the length; these are typically ~1 mm in diameter, spaced 10 mm apart from each other and rotated by 90° hole-to-hole. The benefits of such side holes in commercial polymeric stents due to extraluminal flow, which is complementary to intraluminal flow, has been quantified in both in vivo and in vitro studies, and complemented with numerical simulations [14–18]. These studies also confirmed Poiseuille flow, thus laminar flow, through the long and narrow lumen of the stent. Additionally, the flow rates through modified stents including those with a dual-lumen[19] and 3D printed stents [20] have been studied and compared and analyzed for their drainage performance.

Since flux, which is flow normalized for cross sectional area, is rarely reported, a fair comparison of drainage between the different stent designs is difficult. Similarly, advantages and disadvantages of stiffer versus more flexible stent designs require further analysis. Noteworthy is, however, that an early clinical study comparing stiff and flexible double-J stents of standard designs revealed that stiffer stents resulted in a higher flow resistance [21]. This is an important finding, because for a constant outer diameter, tube stiffness can be reduced and intraluminal flow can be increased through a decrease in tube wall thickness,

while a stiffer material could be used for the stent wall to allow a decrease in stent wall thickness to achieve the same for a retained overall stent stiffness [14]. Finally, an important clinical observation with the current indwelling stiff ureteral stent designs is that, after their placement, the ureter significantly enlarges, enabling significant flow on the stent surface, and that peristalsis is significantly reduced or stopped entirely [22]. Not yet reported in the literature are systematic studies concerning the in vivo performance of flexible or “soft” stents, including their effect on the ureter diameter and peristalsis. Least investigated are porous ureteral stents: the only report in the literature, to date, is the description of a ureteral stent manufactured by a bead-templating method [23]. Entirely absent from the literature, to date, is an analysis and comparison of fluid flow through a porous stent wall with submillimeter-size pores in comparison to a perforated stent with considerably larger ~1 mm diameter holes. This is what we explore in this study.

Porous stents offer alternatives and complement existing solid-walled stent options with the potential for drug release to reduce the pain typically associated with their placement [24–29], which is highly desirable, since intravesical treatment of such pain frequently has relatively limited success[30–34]. Similarly, a porous drug eluting stent could find application for the management of inflammation and short- and long-term cancer therapies. Additional advantages over existing designs are due to a lower stiffness that results in excellent shape conformity and frictional properties, which hold the stent in position, thus without the need of a J-shaped tail, which is known to be the prime cause for patient irritation [35–37]. Similar benefits are expected thanks to improved flow due to the porous stent walls, which is known to reduce the risk of reflux [38].

One way of manufacturing porous stents is freeze-casting, the directional solidification of, most frequently, water-based solutions and slurries followed by lyophilization (freeze drying), resulting in porous materials with a well-defined, highly aligned pore structure and associated anisotropic properties [39–43]. Freeze-casting is a cold, chemically benign process to manufacture porous structures, thus allow several path of incorporating drugs during the process: freezing in small molecules or capsules, soaking in to decorate the cell wall materials, and filling the porosities [44]. The pore alignment is determined by the thermal gradient along which the ice crystals grow. The pore size can be controlled through material composition and processing conditions, the more basic the pH of the polymer solution or slurry and the higher the applied cooling rate, the smaller the pores [41,45]. The pore geometry can be custom-designed through solution or slurry composition and additives, such as ethanol [45–47]. Combined, pore size, geometry, and alignment determine the scaffolds’ mechanical and flow properties. Thus, through the careful choice of solution and slurry composition and processing conditions, stents can be tailor-made for optimized fluid flow on the one hand and appropriate mechanical properties for both surgical handling and patient comfort on the other.

Chitosan is the material of choice for this first exploration of a freeze-cast, porous stent design because it offers additional parameters for the custom-design of scaffold properties: such as the molecular weight and degree of deacetylation. [48–54] Another advantage is that it is a naturally antimicrobial [55,56] and biodegradable [57–59] material, properties that reduce and possibly prevent biofilm formation, preventing stone formation by surface

degradation, enable controlled drug release and enhance penetration, [60–65] and the self-removal of the stent [66–68].

We focus in this study on the microstructure, mechanical properties, and flow characteristics of this newly developed, freeze-cast stent design. Porous chitosan stents were manufactured by freeze-casting using a bi-directional, radial thermal gradient (Figure 1A) [69,70]. The stent microstructures were investigated both in the dry and fully hydrated states. Mechanical properties were evaluated through cyclic loading which mimics the ureter's peristalsis to prove that despite the comparatively low stiffness of the stent, which is expected to increase patient comfort, an open lumen is preserved for urine flow also after severe deformation. Additionally, demonstrated could be the ability of the stent to self-expand, and that the stent stays securely in place after implantation.

The flow performance of the freeze-cast porous chitosan stents was tested in comparison with a standard 8 Fr double-J stent (Universa® Soft Ureteral Stent with Hydrophilic Coating, Cook Medical, Bloomington, IN, USA) using a custom-designed *in vitro* flow testing apparatus (Figure 1B). The flow characteristics (including volumetric flow, Q, flux, V, hydraulic loss, h_f, etc.) of both stent designs, with and without holes, were analyzed assuming a Poiseuille flow pattern.

2. Materials and Methods

2.1. Materials and Reagents

All chemical were used as received: chitosan powder (95% degree deacetylation (DD), 150–350 mPas viscosity for 1% w/v chitosan in 1% acetic acid at 20 °C, as specified by the manufacturer Heppe Medical Chitosan GmbH, Germany; acetic acid (Glacial, ACS grade, EMD Millipore, Burlington, MA, USA); sodium hydroxide (anhydrous, reagent grade), 1-ethyl-3-(3-dimethylaminopropyl) carbodiimide hydrochloride (EDC) and fluorescein sodium salt (all by Sigma-Aldrich, St. Louis, MO, USA); phosphate buffered saline (PBS, biotechnology grade) and 200 Proof ethanol (both by VWR, Radnor, PA, USA).

2.2. Stent Manufacture

Porous chitosan stents were fabricated by injecting 3.5% w/v chitosan in 1.5% v/v acetic acid solution into a mold assembly consisting of an outer aluminum cylinder (3 mm inner diameter; 0.356 mm wall thickness), inner 316 stainless-steel rod (1.5 mm), and custom-designed plastic holders to center the assembly (Figure 1A). The filled molds were placed in a −80 °C freezer (Model 5705, VWR, Radnor, PA, USA) for 20 minutes, gently punched out, and lyophilized for 24 hours (Freezone 6 Plus, Labconco, Kansas City, MO, USA). Once freeze-dried, the porous stents were immersed in 0.4% v/v saturated sodium hydroxide solution in 95% ethanol to neutralize the positive charges, followed by a 6-hour wash in deionized water to remove residual neutralizing solution.

2.3. Microscopy

Transverse and longitudinal sections, inner and outer surfaces of the porous stent, and inner surface of the 8 Fr standard stent were imaged dry and fully hydrated. They were gold

sputtered with a 10 nm thick coating (Hummer 6.2, Anatech, Hayward, CA, USA) for imaging with a scanning electron microscope (Tescan Vega3, Brno-Kohoutovice, Czech Republic). For imaging with a confocal microscope (Nikon A1R, Nikon Instruments Inc., Tokyo, Japan) and 10x lens at 488 nm excitation wavelength, the samples were stained in 0.05 mg mL^{-1} fluorescein sodium salt solution and 0.05 M EDC in PBS for 6 hours at room temperature, followed by three washes in PBS. The dimensions of the porous chitosan stent, 8 Fr stent, and silicone tube were determined by optical microscopy (M205C, Leica Microsystems, Wetzlar, Germany). All measurements on images were conducted using Image J.

2.4. Mechanical Testing

Radial compression testing was performed on an Instron 5498 (Instron, Norwood, MA, USA) with a 50 N load cell and a displacement rate of 0.2 mm s^{-1}. The porous stent (20 mm in length) was fully hydrated in PBS for 24 hours before testing. The fully hydrated porous stent was placed between Teflon coated compression platens; 500 μL PBS were added to keep the stent fully hydrated throughout the testing. The porous stent was compressed radially 100 times to a maximum displacement of 2.4 mm (80% of the porous stent diameter) and unloaded, emulating the regular contractions of peristalsis, which typically occur every 30 s, in humans [71].

The self-expanding and self-stabilizing tests were conducted in vitro using a 1.5 mm diameter stainless steel rod as the guide wire and a silicone tube of 2.65 mm inner diameter to represent the ureter. The porous stent was hydrated and slid into the rod. The water was gently squeezed out with a paper wipe before placing the rod into the tube. The set up was then rinsed with water, and the stainless-steel rod was retracted. This positioning method is analogous to the operative procedure using the clinical double-J stent. The entire process was recorded by a CCD camera (Edge AM3715TB, Dino-Lite, Taipei, Taiwan).

The friction between the porous chitosan stent and the silicone tube was measured in a BioPuls bath (Instron, Norwood, MA, USA) on the Instron. To determine the frictional forces, a porous stent of 60.0 mm length was inserted into the silicone tube for 47.5 mm. The accessible ends of the chitosan stent and the silicone tube, respectively, were glued into plastic straws for gripping to avoid stress concentrations and premature failure at the sample ends. The straws were held in pneumatic grips for testing using a 50 N load cell. Frictional forces were determined until the porous stent started to slide at a displacement rate of 0.01 mm s^{-1} with the sample fully immersed in PBS at 37°C.

2.5. Flow Testing

To compare the flow performance of the porous chitosan with that of the standard 8 Fr stent, both with and without the additional flow paths of pores in the first and side holes in the latter case, 50 mm long sections of each were slid into a silicone tube of 2.65 mm inner diameter and 50 mm length. The silicone tube emulated the ureter and offered conformal contact and minimum strain to the stents positioned inside. Five configurations were tested, the porous stent and 8 Fr stent with and without silicone tubes, respectively, and the silicone tube alone (Figure 1B). Serological pipettes (D = 7.99 mm), with the top cut open to the

atmosphere and bottom trimmed and polished to fit the devices to be tested, were vertically held with a clamp and stand. For testing, the devices were slid into the bottom of the serological pipettes (Figure 1B). The junction was first wrapped with a PTFE film to prevent leakage and additionally sealed by a wider paraffin film to securely connect the silicone tube with the pipette. The setup was rinsed with PBS, capped with a PTFE film at the bottom, and filled with PBS to the 270 mm mark, which falls within the typical pressure range of 18–20 cmH_2O in the healthy human kidney. Once the liquid was static, the bottom cap was removed and the PBS allowed to drain through the respected device. The changes in liquid level were recorded with a high-speed camera (Flare 4M180-CL, IO Industry, London, Canada) at 100 fps. Each device was tested in triplicate.

The energy equation [72] for the liquid column between its top and bottom surfaces of the tested device (position 1 and position 2 in Figure 1B):

$$\frac{p_1}{\rho g} + \frac{\alpha_1 V_1^2}{2g} + z_1 = \frac{p_2}{\rho g} + \frac{\alpha_2 V_2^2}{2g} + z_2 + h_f \quad (1)$$

where

$$V_1 = \frac{4Q}{\pi D^2} \quad (2)$$

and

$$V_2 = \frac{4Q}{\pi d^2} \quad (3)$$

p_1, p_2 are the external pressure, i.e. atmosphere pressure in this case, at position 1 and 2, respectively; V_1 and V_2 are the flux at each position [m s^{-1}]; $z_1$and z_2 are the height of the liquid level; α_1 and α_2 are the kinetic energy correction factors; h_f is the hydraulic (or frictional) loss [m]; Q is the volumetric flow rate [mL s^{-1}]; d is the diameter of the lumen of the tested device (as indicated in in Figure 1B); ρ = 1.01 g mL^{-1} is the density of PBS; g = 9.8 m s^{-2} is the gravitational constant.

To confirm laminar flow (Re < 2000) in the tested devices, the maximum Reynolds number was calculated from the maximum flux V_2, max:

$$Re_{max} = \frac{\rho V_{2,max} d}{\mu} \quad (4)$$

where μ = 1.00 cP is the dynamic viscosity of PBS. Applying Hagen-Poiseuille and Darcy-Weisbach theories for the phenomenological laminar flow and assuming a smooth, circular cross-section of the lumen, the hydraulic losses that encompass the overall resistance to flow can be calculated [72]:

$$h_f = \frac{128\mu LQ}{\pi\rho g d^4} \quad (5)$$

Note that since $D^4 \gg d^4$, only the friction along the tested device, but not the pipette, are taken into account.

To evaluate the effect of stent wall properties on flow — in contrast to earlier studies in which friction losses were evaluated after normalization of the lumen diameter, d [73] — we replaced in Equation 5 the dynamic viscosity μ = 1.00 cP with the effective viscosity μ_{eff}:

$$h_f = \frac{128\mu_{eff} LQ}{\pi\rho g d^4} \quad (6)$$

From the height of the PBS column, h (Figure 1B), determined from every twentieth frame (time difference Δt = 0.2 s) using Image J:

$$h = z_1 - z_2 = \frac{8}{g\pi^2}\left(\frac{-\alpha_1}{D^2} + \frac{\alpha_2}{d^2}\right)Q^2 + \frac{128\mu_{eff} L}{\pi\rho g d^4}Q \quad (7)$$

The corresponding Q was calculated as:

$$\Delta V(t) = 4\pi D^2[h(t - \Delta t) - h(t + \Delta t)] \quad (8)$$

$$Q(t) = \frac{\Delta V(t)}{2\Delta t} \quad (9)$$

The effective viscosity μ_{eff} was calculated from the expression of Equation (6).

The porous chitosan stent (60.0 mm in length) was slid into 100.0 mm silicone tube. The entire section of the porous chitosan stent was accommodated in the peristaltic pump (Figure S1). The pump was running at a moderate speed. The mass of PBS pumped through the pump was measured. An empty silicone tube was tested as control.

3. Results

3.1. Microstructure

The structural analysis of the dried porous stent by SEM revealed an anisotropic architecture with multidomain texture (Figure 2A) and highly aligned, preferentially radially oriented lamellar porosity. The pores closer to the inner and outer stent surfaces were more spherical than lamellar and had shorter pore axes, $s < 25$ μm; they were also smaller in size and more precisely radially aligned than those in the stent wall center, where the structure was more lamellar and the shorter pore axes ranged from 40–60 μm. In contrast to our earlier findings for conduits made by freeze-casting the same chitosan solution between a 4 mm inner

diameter aluminum tube and 2 mm diameter copper rod[69], no distinct membrane that separates the stent wall into an inner and an outer layer was observed. The observed pore structure was preserved also in the fully hydrated state (Figure 2B), however some swelling occurred with the diameter of the porous stents increasing from 2.51 ± 0.05 mm in the dry state to 2.99 ± 0.02 mm in the wet.

Similar size and alignment patterns of the pores were also found in the longitudinal cross-sections of the stents (Figure 2C) Additionally observed were circular and elliptical openings in the cell wall material with diameters of about 20 μm. Both the inner (Figure 2D) and the outer (Figure 2E) surfaces of the stents exhibited porosity; both the overall porosity of the inner surfaces (Figure 2D) was greater with larger individual openings (~50 μm in diameter) than that of the outer surfaces. In comparison, the inner surface of the 8 Fr stent (Figure 2F) was with a roughness <10 μm (the amplitude of surface morphology, estimated based on a comparison with dust particles) considerably smoother than the freeze-cast stent.

3.2. Mechanical Properties

The porous chitosan stent preserved the shape and mechanical properties after 100 loading and release cycles followed by a 30 s dwell time (Figure 3A).

The hysteresis of the five presented cycles after the 1^{st} were almost identical. The maximum load dropped by 7% from 0.86 N to 0.80 N between the 1^{st} and the 100^{th} loading cycle, with the largest drops occurring during the first 40 cycles. To ease sliding the chitosan scaffold into the silicone tube, the water of the fully hydrated chitosan scaffold was gently squeezed out by concentrically pressing against a stainless-steel rod positioned in its lumen. Upon rehydration, the porous chitosan stent expanded and remained in situ in the silicone tube, after the rod was removed (Figure 3B). The static friction force of a 47.5 mm porous stent in the silicone tube was measure to be 321 mN and with it the static friction per unit length determined to be 67.6 mN mm^{-1}.

3.3. Flow Characteristics

Both the porous chitosan stents and the standard stents exhibit a higher flux for the entire pressure range when not placed in the silicone tube (Figure 4). The flux in the porous chitosan stents was lower than that of the commercial stents, both when placed in the silicone tube, and when not. Neither the porous stent nor the 8 Fr stent migrated in the silicone tube before, during, or after fluid drainage.

The Reynolds numbers Re calculated from the maximum flux in each case <2000 for all stent designs (Table 1) confirming laminar flow; it was >2000, and thus in transition to turbulent, only in the case of empty silicone tube, in which the highest flux was observed among all.

The effective viscosities μ_{eff} for each stent design and configuration were calculated assuming the laminar flow (Table 1). The effective viscosities decreased in the following order: porous stent with tube, porous stent without tube, commercial 8 Fr stent with tube and commercial 8 Fr stent without tube. The porous chitosan stents had larger effective viscosities than the 8 Fr stents, both when placed in the silicone tube, and when not. Both

the 8 Fr stent and porous stent showed higher effective viscosities when tested in the silicone tube: the effective viscosities decreased by 30.6 % for the commercial stent and by 47.5% for the porous stent, upon removal of the silicone tube.

Flow tests were performed in a peristaltic pump with a 3 mm outer and 1.52 mm inner diameter porous chitosan stent of 96% overall porosity inserted into a model ureter represented by a 2.65 mm diameter silicone tube and, for comparison, an empty silicone tube. The volumetric flow rate of the silicone tube with the porous stent present was 13.68 mL min^{-1} or 88% of hat without 15.47 mL min^{-1}; the silicone tube did not dilate passively (Supplementary Video 1).

4. Discussion

4.1. Stent Microstructure

The thin layer of cellular porosity observed adjacent to both the inner and outer stent surfaces, were formed by the initially high density of ice nuclei that form due to the high undercooling in the −80°C freezer at the beginning of the freezing process [74]. Increasingly, favorably oriented crystals dominate crystal growth, the thermal gradient decreases in the mold, slowing the growth rate towards the center. The result are larger, less aligned pores in the center of the stent wall.

Freeze-cast tubular structures were also fabricated by a spinning technique offering intimate contact between the outer surface and the coolant; this resulted in smaller pores at the outside layer and highly radially aligned pores[75–78]. The mechanical properties of the structure in this study likely benefits from a higher number of domains that support each other as oppose to a radially aligned porous structure with few domains.

Noteworthy is that in contrast to the porous tubular structure of an earlier study, which had twice the thickness[69], no central membrane was observed, This is likely due to the fact that the center of the thinner layer of the chitosan solution can cool considerably faster, so that the stent solidifies before a quasi-steady regime of solidification, which is required for the membrane formation, can be reached [79]. As a result, no distinctive membrane forms, where the two freezing fronts meet.

4.2. Mechanical Properties

Two attractive stent properties were observed during mechanical testing: the ability to conform to the silicone tube, which emulated the ureter, and an elastic and resilient response. Under cyclic loading, which mimicked the frequency and dwell time of peristalsis, the porous chitosan stent deformed and reliably recovered after 100 cycles with 7% drop in strength. The two regions of the loading curve of different modulus agreed with the previous observations of similar tubular scaffold [69]. No plastic collapse was observed, however a slightly increased permanent plastic deformation, which decreases with increasing loading cycles, is expected for more extended cyclic loading. The load required to achieve a displacement of 2.4 mm, which is 80% of the diameter of the porous stent, was less than 1 N, indicating the low stiffness of the highly porous, but resilient stent, which fully recovers its shape upon removal of the load. Thus, the porous stents were soft but durable. The

"softer" feel is expected to improve patient comfort after implantation. The resilience of the chitosan structure also resulted in a shape conforming [80] effect, which allowed the stent to remain in place during fluid flow by exerting radial forces on the silicone tube side walls. We anticipate this mechanism of stabilization and biopolymer conformity in tubular structures [81] to translate to the ureter thereby eliminating the need for the double-J design in current clinical devices.

4.3. Flow Characteristics

The 8 Fr stent had millimeter size side holes along the length to serve as additional pathways for flow [82]. As one of the first porous ureteral stents, the porous chitosan stents of this study have highly aligned radial porosity through the stent wall, which, we believe, aid flow as effectively as the side holes in the standard 8 Fr stent. The aligned porosity it thought to guide the radial flow across the wall eliminating the longitudinal flow within the stent wall, thus increasing the extraluminal flow[83,84]. The higher flux through the 8 Fr stents compared to that of the porous chitosan stents can be attributed to their large lumen diameter.

For a fair comparison solely between the device designs, which include material choice and geometric properties of the stent wall, but not the effect of absolute stent dimensions, a non-dimensional parameter independent of the stent diameter was calculated, μ^*, which describes the effective viscosity. The difference in effective viscosity for the different designs illustrates differences in interactions between the liquid and the stent wall. The higher effective viscosity measured in the freeze-cast stent is likely due to the larger and more irregular roughness of the inner stent surface, which causes local turbulences in the flow.

The observed decrease in effective viscosities in all stent designs upon the removal of the silicone tube were likely due to the outside stent surface offering a new, additional path for flow leading to improved drainage. The comparison of the effective viscosity of the five different stent types and wall designs was used to evaluate their respective effectiveness to promote flow. A larger decrease (48%) in the effective viscosity of the porous chitosan stents after tube removal in comparison to the 8 Fr stent (31%) suggests that their radially aligned pores function as 'side holes' facilitating a superior flow performance. In addition to the demonstrated benefits that the radial porosity of the freeze-cast stents provides in its current form, namely a symmetrical pore geometry, in which the pore diameter increases from the stent wall surfaces to the center of the wall, it will be interesting to investigate, benefits of asymmetric pore geometries. A decrease in pore diameter from the outside to the inside wall surface, for example, might increase flow into the lumen, taking advantage of capillarity as demonstrated in ceramic scaffolds [75]. Further studies are required to explore such effects systematically and determine structure-property-processing correlations for freeze-cast tubular structure and the resulting drainage properties.

The in vitro testing of the flow through a porous stent in a model ureter in a peristaltic pump demonstrates its capability of draining with 88% of flow in comparison to the empty model ureter, assuming that the porous stent does not lead to a dilatation of the ureter.

4.4. Clinical Relevance

Ureteral stent design requirements are not universal, but depend on a given indication. Keeping the ureter patent in the presence of an extrinsic/intrinsic stricture such as a tumor or malignancy, for example, requires such a high lateral stiffness of the tube to prevent ovalization and collapse that successful stents for this application can only be made from metals due to their intrinsic materials stiffness, i.e. their high Young's modulus, *E*. The desired ease of placement and removal of the stent and patient comfort puts practical upper and lower limits on the longitudinal stiffness of the stent, which is described by their product, *EI,* and determined by both the stent material (through its intrinsic material stiffness, *E)* and tube geometry (the stent's second moment of area, *I*, which for a tubular stent is defined by the tube radius and the tube wall thickness).

Porous stents such as the one assessed in this study are promising alternatives to the current double-J stend models, not only, because they can be custom-designed but also, because they ideally lend themselves for systematic studies to determined yet little-explored correlations. The custom-design of material properties and architecture allows, for example, to obtain the required lateral and longitudinal stiffness and strength, and the respective surface and flow characteristics. They are also a good model with which to explore correlations between stent-stiffness, ureter dilatation, and peristalsis, and the effect of biodegradation on biofilm formation and encrustation. Finally, they are well suited for local short- and longer-term drug delivery for reduced pain, irritation, and cancer therapies.

A large range of stent material-architecture combinations is commercially available; standard stents are mostly made from polymers, which are highly biocompatible and sometimes also biodegradable, and have a double-J tail design to secure the stent in place. This standard stent design is sometimes modified to include, for examples, holes or a mesh or a spiral architecture, for improved drainage. However, in their bare form, many of the polymeric and metal stents a prone to biofilm formation and encrustation.

Both biofilm formation and encrustation, which must ideally be avoided or at least be delayed and minimized to avoid complications such as inflammation and stone formation, and possible reduced drainage, are encouraged or discouraged by the stent's surface chemistry and topography. At the same time, surface chemistry and topography also affect stent wettability and fluid flow dynamics, and through these, again, biofilm formation and encrustation. While surface coatings and drug-eluting stent materials can be introduced to reduce these risks, no true optimal stent design exists that simultaneously satisfies all of the key design requirements.

Clinicians report that, despite the existence of a considerable number of material-architecture-surface property combinations that are currently available for application in the clinic, none of the current designs are truly ideal; there is a desire for alternatives with improved performance, and for stents that offer properties which go beyond those currently available. Desirable would be, in addition to truly fully biodegradable designs that would eliminate complications associated with forgotten stents, also stents with considerably increased patient comfort. Designs that would reduce or eliminate the frequently encountered irritations, which are mostly caused by the current J-tail would achieve the

latter goal. Of similar merit would be stents that offer significantly improved pain management and cancer therapy options, through short- and long-term drug release.

Noteworthy with respect to functionality is that in the current double-J stent designs the majority of urine can flow on the outside of the stent rather than through the lumen, because the placement of a double-J stent and the resulting partial blockage of the lumen causes a passive ureteric dilatation by about 1.5 to 2 times from a typical ureter diameter of 1–2 mm (3–6 Fr) to about 2–4 mm (6–12 Fr) in response to the stent placement. It appears that the passive dilatation of the ureter after the placement of a stent in vivo is due to an increase in flow resistance that is caused by the reduction in lumen diameter and cross-section; since the flow resistance increases with the power of 4 with a decrease in lumen radius (see for example equation 7), a seemingly small lumen diameter reduction has a considerable effect on the flow dynamics. The considerable passive dilatation response to the stent placement is frequently utilized to obtain a ureter of sufficient diameter for a second procedure to be performed using a ureteroscope naked over a guidewire or an access sheath that has been placed in the desired position.

Not reported in the literature to date is the response to a porous and compressible stent, which conforms with the ureter at all times, without dilating it. The authors hypothesize that the response to a compliant porous stent might be continued peristalsis, and therefore performed flow tests with a 3 mm outer and 1.52 mm inner diameter porous chitosan stent with 96% overall porosity, and compared flow through a model ureter, represented by a 2.65 mm diameter silicone tube, in both its presence and its absence. The volumetric flow rate of the silicone tube with the porous stent present was 88% that of the unstented silicone tube, which did not dilate passively, as reported above.

While the authors consider this result highly promising for the flow performance of the porous stent, they consider it premature to make predictions as to its in vivo performance, since there is currently no data on the basis of which it would be possible to anticipate whether a compliant, compressible stent that deforms along with the ureter during peristalsis, might cause the same passive ureteric dilatation as the stiff standard stent of current practice.

Last, but not least, it appears that the porous stent design holds promise for reduced morbidity for the following reasons. The antimicrobial properties of chitosan itself reported in the literature, is expected to help reduce, possibly even eliminate entirely the need for surface modification [85] or drug elution [66] to prevent biofilm formation, stone formation, and infection [86,87]. Chitosan’s biodegradability, which can be controlled, for example, through the choice of molecular weight and degree of deacetylation, is additionally expected to enhance the materials antimicrobial performance, and to prevent the nucleation and growth of stones to a critical size by continuously shedding surface material. The biodegradation of chitosan has been reported to be consistent, meaning uniform and without the production of fragments that could obstruct urine flow [59]. Optimization of the biodegradability of chitosan will also allow for a biodegradable stent design for self-removal after a clinically relevant timeframe, avoiding forgotten stent morbidity, which cannot only lead to potential kidney loss but even death [88].

Finally, the porous design and drug loading capability of chitosan [61,62] are highly promising as a means to enhance the functionality of porous stent for pain management and even cancer therapy, for which no truly satisfactory solution for longer-term drug release currently exists in the clinic [30–32]. Further research, beyond the scope of this study, will be required to assess systematically in vitro and in vivo biodegradability, antimicrobial properties, and drug release efficacy of the porous stents. The exploration of these properties is beyond the scope of this first exploratory study as a proof of concept of a new biomaterial and one possible application.

5. Conclusion

The newly designed porous chitosan ureteral stent design was manufactured from chitosan by radial, bi-directional freeze-casting. The resulting structure had radially aligned pores organized in domains, with smaller, better aligned pores closer to the surfaces from which the solidification started. The stent was shown to be elastic and resilient; it self-expanded and remained safely positioned in the silicone urinary track mimic during the flow tests. Emulating peristalsis by cyclic loading for up to 100 cycles, the maximum load dropped by 7%, however, no significant permanent deformation was observed in the stent. While displaying a lower *in vitro* flux, the performance of the porous chitosan stent improves considerably more (47.5%) than that of the 8 Fr stent (30.6%) upon removal from the tube, illustrating the effectiveness of the radially aligned porosity for drainage. With the observed drainage performance and additional benefits of biodegradability, antimicrobial properties, drug release, and potentially improved patient comfort due to a lower stiffness than current commercial designs, we conclude that porous chitosan stents are highly attractive candidates for ureteral stenting

Supplementary Material

Refer to Web version on PubMed Central for supplementary material.

Acknowledgements

The authors gratefully acknowledge financial support through NIH-NICHD Award R21HD087828 and NSF-CMMI Award 1538094 and would like to thank Dr. Kevin J. Krughoff, Prof. David R. Chavez and Prof. Frank Penna, MD, all Pediatric Urologist at Dartmouth College and Prof. Brenden Epps, Thayer School of Engineering at Dartmouth College for stimulating discussions, and the Dartmouth College Electron Microscopy facilities for their expert support.

References

[1]. Marieb EN, Hoehn KN, Anatomy & Physiology, Pearson Education, 2016.

[2]. Chang R, Marshall FF, Mitchell S, Percutaneous Management of Benign Ureteral Strictures and Fistulas, J. Urol. 137 (1987) 1126–1131. doi:10.1016/S0022-5347(17)44426-0. [PubMed: 3586141]

[3]. Ilie VG, Ilie VI, Ureteric Stent Use - Part of the Solution and Part of the Problem, Curr. Urol. 11 (2017) 126–130. doi: 10.1159/000447206.

[4]. Dyer RB, Chen MY, Zagoria RJ, Regan JD, Hood CG, Kavanagh PV, Complications of Ureteral Stent Placement, RadioGraphics. 22 (2002) 1005–1022. doi :10.1148/radiographics.22.5.g02se081005. [PubMed: 12235330]

[5]. MPN, Ureteral Stents Improving Comfort, Safety and Efficacy, Med. Plast. News. (2014). https://www.medicalplasticsnews.com/api/content/02d423fc-89c7-11e3-bbdc-1231380a02d9/(accessed March 27, 2018).

[6]. Kulkarni R, Ureteric Stenting, John Wiley & Sons, 2017.

[7]. Ho C-H, Huang K-H, Chen S-C, Pu Y-S, Liu S-P, Yu H-J, Choosing the Ideal Length of a Double-Pigtail Ureteral Stent according to Body Height: Study Based on a Chinese Population, Urol. Int. 83 (2009) 70–74. doi:10.1159/000224872. [PubMed: 19641363]

[8]. Pilcher JM, Patel U, Choosing the correct length of ureteric stent: a formula based on the patient's height compared with direct ureteric measurement, Clin. Radiol. 57 (2002) 59–62. doi: 10.1053/crad.2001.0737. [PubMed: 11798204]

[9]. Palmer JS, Palmer LS, Determining the proper stent length to use in children: age plus 10, J. Urol. 178 (2007) 1566–1569. doi:10.1016/j.juro.2007.03.191.

[10]. Erturk E, Sessions A, Joseph JV, Impact of ureteral stent diameter on symptoms and tolerability, J. Endourol. 17 (2003) 59–62. doi:10.1089/08927790360587342. [PubMed: 12689395]

[11]. Damiano R, Autorino R, De Sio M, Cantiello F, Quarto G, Perdonà S, Sacco R, D'Armiento M, Does the size of ureteral stent impact urinary symptoms and quality of life? A prospective randomized study, Eur. Urol. 48 (2005) 673–678. doi:10.1016/j.eururo.2005.06.006. [PubMed: 16039775]

[12]. Candela JV, Bellman GC, Ureteral stents: impact of diameter and composition on patient symptoms, J. Endourol. 11 (1997) 45–47. doi:10.1089/end.1997.11.45. [PubMed: 9048298]

[13]. Stents: Ureteral, Boston Sci. (n.d.). http://www.bostonscientific.com/en-US/products/stents–ureteral.html.

[14]. Brewer AV, Elbahnasy AM, Bercowsky E, Maxwell KL, Shalhav AL, Kahn SA, McDougall EM, Clayman RV, Mechanism of ureteral stent flow: A comparative in vivo study, J. Endourol. 13 (1999) 269–271. doi:10.1089/end.1999.13.269. [PubMed: 10405904]

[15]. Kim HH, Choi YH, Lee SB, Baba Y, Kim KW, Suh SH, Numerical of the urine flow in a stented ureter with no peristalsis, Biomed. Mater. Eng. 26 (2015) S215–S223. doi:10.3233/BME-151308. [PubMed: 26405994]

[16]. Kim HH, Choi YH, Lee SB, Baba Y, Kim KW, Suh SH, Numerical analysis of urine flow through the side holes of a double J stent in a ureteral stenosis, Technol. Health Care. 25 (2017) 63–72. doi:10.3233/THC-171307. [PubMed: 28582893]

[17]. Lowe D, Hafron JM, Davelman FS, Desai AS, Hoenig DM, Flow characteristics of a 4.2 F ureteral stent compared to a standard 7 F ureteral stent in an ex vivo porcine kidney model, J. Endourol. 20 (2006) A187–A187.

[18]. Blaschko SD, Deane LA, Krebs A, Abdelshehid CS, Khan F, Borin J, Nguyen A, McDougall EM, Clayman RV, In-Vivo Evaluation of Flow Characteristics of Novel Metal Ureteral Stent, J. Endourol. 21 (2007) 780–783. doi:10.1089/end.2006.0315. [PubMed: 17705771]

[19]. Hafron J, Ost MC, Tan BJ, Fogarty JD, Hoenig DM, Lee BR, Smith AD, Novel dual-lumen ureteral stents provide better ureteral flow than single ureteral stent in ex vivo porcine kidney model of extrinsic ureteral obstruction, Urology. 68 (2006) 911–915. doi:10.1016/j.urology.2006.05.025. [PubMed: 17070391]

[20]. del Junco M, Yoon R, Okhunov Z, Abedi G, Hwang C, Dolan B, Landman J, Comparison of Flow Characteristics of Novel Three-Dimensional Printed Ureteral Stents Versus Standard Ureteral Stents in a Porcine Model, J. Endourol. 29 (2015) 1065–1069. doi:10.1089/end.2014.0716. [PubMed: 26196704]

[21]. Hübner WA, Plas EG, Stoller ML, The Double-J Ureteral Stent: In Vivo and in Vitro Flow Studies, J. Urol. 148 (1992) 278–280. doi:10.1016/S0022-5347(17)36572-2. [PubMed: 1635117]

[22]. Venkatesh R, Landman J, Minor SD, Lee DI, Rehman J, Vanlangendonck R, Ragab M, Morrissey K, Sundaram CP, Clayman RV, Impact of a Double-Pigtail Stent on Ureteral Peristalsis in the Porcine Model: Initial Studies Using a Novel Implantable Magnetic Sensor, J. Endourol. 19 (2005) 170–176. doi:10.1089/end.2005.19.170. [PubMed: 15798413]

[23]. Davoudi H, Intoccia A, Li J, Porous ureteral stent, US8414656B2, 2013.

[24]. Koprowski C, Kim C, Modi PK, Elsamra SE, Ureteral Stent-Associated Pain: A Review, J. Endourol. 30 (2016) 744–753. doi:10.1089/end.2016.0129. [PubMed: 27125392]

[25]. Walker NAF, Bultitude MF, Brislane K, Thomas K, Glass JM, Management of stent symptoms: what a pain!, BJU Int. 114 (2014) 797–798. doi :10.1111/bju.12534. [PubMed: 25216234]

[26]. Sivalingam S, Monga M, Management of Ureteral Stent Discomfort in Contemporary Urology Practice, Urol. Pract. 1 (2014) 141–145. doi:10.1016/j.urpr.2014.06.001.

[27]. Olweny EO, Portis AJ, Sundaram CP, Afane JS, Humphrey PA, Ewers R, McDougall EM, Clayman RV, Evaluation of a chronic indwelling prototype mesh ureteral stent in a porcine model, Urology. 56 (2000) 857–862. doi:10.1016/S0090-4295(00)00734-2. [PubMed: 11068323]

[28]. Joshi HB, Stainthorpe A, Keeley FX, MacDonagh R, Timoney AG, Indwelling ureteral stents: evaluation of quality of life to aid outcome analysis, J. Endourol. 15 (2001) 151–154. doi: 10.1089/089277901750134421. [PubMed: 11325084]

[29]. Joshi HB, Stainthorpe A, MacDONAGH RP, Keeley FX, Timoney AG, Indwelling Ureteral Stents: Evaluation of Symptoms, Quality of Life and Utility, J. Urol. 169 (2003) 1065–1069. doi: 10.1097/01.ju.0000048980.33855.90. [PubMed: 12576847]

[30]. Beiko DT, Watterson JD, Knudsen BE, Nott L, Pautler SE, Brock GB, Razvi H, Denstedt JD, Second Prize: Double-Blind Randomized Controlled Trial Assessing the Safety and Efficacy of Intravesical Agents for Ureteral Stent Symptoms after Extracorporeal Shockwave Lithotripsy, J. Endourol. 18 (2004) 723–730. doi:10.1089/end.2004.18.723. [PubMed: 15659891]

[31]. GuhaSarkar S, Banerjee R, Intravesical drug delivery: Challenges, current status, opportunities and novel strategies, J. Control. Release Off. J. Control. Release Soc. 148 (2010) 147–159. doi: 10.1016/j.jconrel.2010.08.031.

[32]. Sur RL, Haleblian GE, Cantor DA, Springhart WP, Albala DM, Preminger GM, Efficacy of intravesical ropivacaine injection on urinary symptoms following ureteral stenting: a randomized, controlled study, J. Endourol. 22 (2008) 473–478. doi:10.1089/end.2007.9847. [PubMed: 18290733]

[33]. Dellis A, Joshi HB, Timoney AG, Keeley FX, Relief of Stent Related Symptoms: Review of Engineering and Pharmacological Solutions, J. Urol. 184 (2010) 1267–1272. doi:10.1016/j.juro. 2010.06.043. [PubMed: 20723923]

[34]. Norris RD, Sur RL, Springhart WP, Marguet CG, Mathias BJ, Pietrow PK, Albala DM, Preminger GM, A Prospective, Randomized, Double-Blinded Placebo-Controlled Comparison of Extended Release Oxybutynin Versus Phenazopyridine for the Management of Postoperative Ureteral Stent Discomfort, Urology. 71 (2008) 792–795. doi:10.1016/j.urology.2007.11.004. [PubMed: 18339420]

[35]. Lingeman JE, Preminger GM, Goldfischer ER, Krambeck AE, Assessing The Impact Of Ureteral Stent Design On Patient Comfort, J. Urol. 181 (2009) 2581–2587. doi:10.1016/j.juro. 2009.02.019. [PubMed: 19375088]

[36]. Thomas R, Indwelling ureteral stents: impact of material and shape on patient comfort, J. Endourol. 7 (1993) 137–140. doi:10.1089/end.1993.7.137. [PubMed: 8518826]

[37]. Betschart P, Zumstein V, Piller A, Schmid H-P, Abt D, Prevention and treatment of symptoms associated with indwelling ureteral stents: A systematic review, Int. J. Urol. 24 (2017) 250–259. doi:10.1111/iju.13311. [PubMed: 28236323]

[38]. Cummings LJ, Waters SL, Wattis J. a. D., Graham SJ, The effect of ureteric stents on urine flow: reflux, J. Math. Biol. 49 (2004) 56–82. doi:10.1007/s00285-003-0252-4. [PubMed: 15235819]

[39]. Wegst UGK, Bai H, Saiz E, Tomsia AP, Ritchie RO, Bioinspired structural materials, Nat. Mater. 14 (2015) 23–36. doi:10.1038/nmat4089. [PubMed: 25344782]

[40]. Deville S, Saiz E, Nalla RK, Tomsia AP, Freezing as a Path to Build Complex Composites, Science. 311 (2006) 515–518. doi:10.1126/science.1120937. [PubMed: 16439659]

[41]. Wegst UGK, Schecter M, Donius AE, Hunger PM, Biomaterials by freeze-casting, Philos. Trans. R. Soc. Math. Phys. Eng. Sci. 368 (2010) 2099–2121. doi:10.1098/rsta.2010.0014.

[42]. Meghri NW, Donius AE, Riblett BW, Martin EJ, Clyne AM, Wegst UGK, Directionally solidified biopolymer scaffolds: Mechanical properties and endothelial cell responses, JOM. 62 (2010) 71–75. doi:10.1007/s11837-010-0112-9. [PubMed: 21544225]

[43]. Divakar P, Yin K, Wegst UGK, Anisotropic Freeze-Cast Collagen Scaffolds for Tissue Regeneration: How Processing Conditions Affect Structure and Properties in the Dry and Fully Hydrated States, J. Mech. Behav. Biomed. Mater. (2018).

[44]. Francis NL, Hunger PM, Donius AE, Wegst UGK, Wheatley MA, Strategies for neurotrophin-3 and chondroitinase ABC release from freeze-cast chitosan–alginate nerve-guidance scaffolds, J. Tissue Eng. Regen. Med. 11 (2017) 285–294. doi:10.1002/term.1912. [PubMed: 24889394]

[45]. Riblett BW, Francis NL, Wheatley MA, Wegst UGK, Ice-Templated Scaffolds with Microridged Pores Direct DRG Neurite Growth, Adv. Funct. Mater. 22 (2012) 4920–4923. doi:10.1002/adfm.201201323.

[46]. Möllers S, Heschel I, Damink LHHO, Schügner F, Deumens R, Müller B, Bozkurt A, Nava JG, Noth J, Brook GA, Cytocompatibility of a Novel, Longitudinally Microstructured Collagen Scaffold Intended for Nerve Tissue Repair, Tissue Eng. Part A. 15 (2008) 461–472. doi:10.1089/ten.tea.2007.0107.

[47]. Hunger PM, Donius AE, Wegst UGK, Structure–property-processing correlations in freeze- cast composite scaffolds, Acta Biomater. 9 (2013) 6338–6348. doi:10.1016/j.actbio.2013.01.012. [PubMed: 23321303]

[48]. Foster LJR, Ho S, Hook J, Basuki M, Marçal H, Chitosan as a Biomaterial: Influence of Degree of Deacetylation on Its Physiochemical, Material and Biological Properties, PLOS ONE. 10 (2015) e0135153. doi:10.1371/journal.pone.0135153.

[49]. Prasitsilp M, Jenwithisuk R, Kongsuwan K, Damrongchai N, Watts P, Cellular responses to chitosan in vitro: The importance of deacetylation, J. Mater. Sci. Mater. Med. 11 (2000) 773–778. doi: 1008997311364. [PubMed: 15348059]

[50]. Chen RH, Hwa H-D, Effect of molecular weight of chitosan with the same degree of deacetylation on the thermal, mechanical, and permeability properties of the prepared membrane, Carbohydr. Polym. 29 (1996) 353–358. doi:10.1016/S0144-8617(96)00007-0.

[51]. Kingkaew J, Kirdponpattara S, Sanchavanakit N, Pavasant P, Phisalaphong M, Effect of molecular weight of chitosan on antimicrobial properties and tissue compatibility of chitosan-impregnated bacterial cellulose films, Biotechnol. Bioprocess Eng. 19 (2014) 534–544. doi:10.1007/s12257-014-0081-x.

[52]. Hamilton V, Yuan Y, Rigney DA, Puckett AD, Ong JL, Yang Y, Elder SH, Bumgardner JD, Characterization of chitosan films and effects on fibroblast cell attachment and proliferation, J. Mater. Sci. Mater. Med. 17 (2006) 1373–1381. doi:10.1007/s10856-006-0613-9. [PubMed: 17143770]

[53]. Jennings JA, Bumgardner JD, Chitosan Based Biomaterials Volume 1: Fundamentals, Elsevier Science & Technology, 2016.

[54]. Chen X-G, Zheng L, Wang Z, Lee C-Y, Park H-J, Molecular Affinity and Permeability of Different Molecular Weight Chitosan Membranes, J. Agric. Food Chem. 50 (2002) 5915–5918. doi:10.1021/jf020151g. [PubMed: 12358459]

[55]. Liu X, Guan Y, Yang D, Li Z, Yao D, Antibacterial action of chitosan and carboxymethylated chitosan, J. Appl. Polym. Sci. 79 (2001) 1324–1335. doi:AID-APP210>3.0.C0;2-L.

[56]. Jeon SJ, Oh M, Yeo W-S, Galvão KN, Jeong KC, Underlying Mechanism of Antimicrobial Activity of Chitosan Microparticles and Implications for the Treatment of Infectious Diseases, PLoS One. 9 (2014) e92723. doi:10.1371/journal.pone.0092723.

[57]. Ren D, Yi H, Wang W, Ma X, The enzymatic degradation and swelling properties of chitosan matrices with different degrees of N-acetylation, Carbohydr. Res. 340 (2005) 2403–2410. doi:10.1016/j.carres.2005.07.022. [PubMed: 16109386]

[58]. Agnihotri SA, Kulkarni VD, Kulkarni AR, Aminabhavi TM, Degradation of chitosan and chemically modified chitosan by viscosity measurements, J. Appl. Polym. Sci. 102 (2006) 3255–3258. doi:10.1002/app.24663.

[59]. Szymańska E, Winnicka K, Stability of Chitosan—A Challenge for Pharmaceutical and Biomedical Applications, Mar. Drugs. 13 (2015) 1819–1846. doi:10.3390/md13041819. [PubMed: 25837983]

[60]. Rinaudo M, Chitin and chitosan: Properties and applications, Prog. Polym. Sci. 31 (2006) 603–632. doi :10.1016/j.progpolymsci.2006.06.001.

[61]. Bhattarai N, Gunn J, Zhang M, Chitosan-based hydrogels for controlled, localized drug delivery, Adv. Drug Deliv. Rev. 62 (2010) 83–99. doi:10.1016/j.addr.2009.07.019. [PubMed: 19799949]

[62]. Bernkop-Schnürch A, Dünnhaupt S, Chitosan-based drug delivery systems, Eur. J. Pharm. Biopharm. 81 (2012) 463–469. doi:10.1016/j.ejpb.2012.04.007. [PubMed: 22561955]

[63]. Erman A, Kos M. Kerec, Žakelj S, Resnik N, Romih R, Veranič P, Correlative study of functional and structural regeneration of urothelium after chitosan-induced injury, Histochem. Cell Biol. 140 (2013) 521–531. doi:10.1007/s00418-013-1088-7. [PubMed: 23553328]

[64]. Višnjar T, Kreft ME, The complete functional recovery of chitosan-treated biomimetic hyperplastic and normoplastic urothelial models, Histochem. Cell Biol. 143 (2015) 95–107. doi:10.1007/s00418-014-1265-3. [PubMed: 25161121]

[65]. Pick DL, Shelkovnikov S, Canvasser N, Louie MK, Tongson-Ignacio J, McDougall EM, Clayman RV, First prize: Chitosan and the urothelial barrier: effects on ureteral intraluminal drug penetration and peristalsis, J. Endourol. 25 (2011) 385–390. doi:10.1089/end.2010.0205. [PubMed: 21126192]

[66]. Barros AA, Browne S, Oliveira C, Lima E, Duarte ARC, Healy KE, Reis RL, Drug-eluting biodegradable ureteral stent: New approach for urothelial tumors of upper urinary tract cancer, Int. J. Pharm. 513 (2016) 227–237. doi:10.1016/j.ijpharm.2016.08.061. [PubMed: 27590593]

[67]. Barros AA, Oliveira C, Lima E, Duarte ARC, Reis RL, Gelatin-based biodegradable ureteral stents with enhanced mechanical properties, Appl. Mater. Today. 5 (2016) 9–18. doi:10.1016/j.apmt.2016.07.006.

[68]. Chew BH, Lange D, Paterson RF, Hendlin K, Monga M, Clinkscales KW, Shalaby SW, Hadaschik BA, Next generation biodegradable ureteral stent in a yucatan pig model, J. Urol. 183 (2010) 765–771. doi:10.1016/j.juro.2009.09.073. [PubMed: 20022028]

[69]. Yin K, Divakar P, Hong J, Moodie KL, Rosen JM, Sundback CA, Matthew MK, Wegst UGK, Freeze-cast Porous Chitosan Conduit for Peripheral Nerve Repair, MRS Adv. 3 (2018) 1677–1683. doi:10.1557/adv.2018.194. [PubMed: 30009044]

[70]. Mohan S, Hernández IC, Wang W, Yin K, Sundback CA, Wegst UGK, Jowett N, Fluorescent Reporter Mice for Nerve Guidance Conduit Assessment: A High-Throughput in vivo Model, The Laryngoscope. (2018). doi:10.1002/lary.27439.

[71]. Griffiths DJ, Flow of Urine Through the Ureter: A Collapsible, Muscular Tube Undergoing Peristalsis, J. Biomech. Eng. 111 (1989) 206–211. doi:10.1115/1.3168367. [PubMed: 2779185]

[72]. White FM, Fluid Mechanics, 8th ed., McGraw-Hill Education, 2016 https://www.mheducation.com/highered/product/fluid-mechanics-white/M0073398276.html (accessed March 9, 2018).

[73]. Olweny EO, Portis AJ, Afane JS, Brewer AV, Shalhav AL, Luszczynski K, McDougall EM, Clayman RV, Flow Characteristics of 3 Unique Ureteral Stents: Investigation of a Poiseuille Flow Pattern, J. Urol. 164 (2000) 2099–2103. doi:10.1016/S0022-5347(05)66977-7. [PubMed: 11061935]

[74]. Deville S, Saiz E, Tomsia AP, Freeze-casting of hydroxyapatite scaffolds for bone tissue engineering, Biomaterials. 27 (2006) 5480–5489. doi:10.1016/j.biomaterials.2006.06.028. [PubMed: 16857254]

[75]. Bai H, Wang D, Delattre B, Gao W, Coninck JD, Li S, Tomsia AP, Biomimetic gradient scaffold from ice-templating for self-seeding of cells with capillary effect, Acta Biomater. 20 (2015) 113–119. doi:10.1016/j.actbio.2015.04.007. [PubMed: 25871536]

[76]. Harley BA, Hastings AZ, Yannas IV, Sannino A, Fabricating tubular scaffolds with a radial pore size gradient by a spinning technique, Biomaterials. 27 (2006) 866–874. doi:10.1016/j.biomaterials.2005.07.012. [PubMed: 16118016]

[77]. Seuba J, Leloup J, Richaud S, Deville S, Guizard C, Stevenson AJ, Fabrication of ice-templated tubes by rotational freezing: Microstructure, strength, and permeability, J. Eur. Ceram. Soc. 37 (2017) 2423–2429. doi:10.1016/j.jeurceramsoc.2017.01.014.

[78]. Wang C, Chen X, Wang B, Huang M, Wang B, Jiang Y, Ruoff RS, Freeze-Casting Produces a Graphene Oxide Aerogel with a Radial and Centrosymmetric Structure, ACS Nano. (2018). doi:10.1021/acsnano.8b01747.

[79]. Leloup J, Gauthier C, Deville S, Bogner A, Maire E, Guizard C, Bernard-Granger G, Lasalle A, Metastable and unstable cellular solidification of colloidal suspensions, Nat. Mater. 8 (2009) 966–972. doi:10.1038/nmat2571. [PubMed: 19898459]

[80]. Lauto A, Ohebshalom M, Esposito M, Mingin J, Li PS, Felsen D, Goldstein M, Poppas DP, Self-expandable chitosan stent: design and preparation, Biomaterials. 22 (2001) 1869–1874. doi : 10.1016/S0142-9612(00)00371-9. [PubMed: 11396892]

[81]. Divakar P, Caruso I, Moodie KL, Theiler RN, Hoopes PJ, Wegst UGK, Design, Manufacture, and In vivo Testing of a Tissue Scaffold for Permanent Female Sterilization by Tubal Occlusion, MRS Adv. 3 (2018) 1685–1690. doi:10.1557/adv.2018.57. [PubMed: 30416761]

[82]. Kim KW, Choi YH, Lee SB, Baba Y, Kim HH, Suh SH, Numerical analysis of the effect of side holes of a double J stent on flow rate and pattern, Biomed. Mater. Eng. 26 Suppl 1 (2015) 319. doi:10.3233/BME-151319.

[83]. Zeman LJ, Zydney AL, Microfiltration and ultrafiltration :principles and applications, Marcel Dekker, New York, 1996.

[84]. Chang C-J, Hsu S, The effect of high outflow permeability in asymmetric poly(dl-lactic acid-co-glycolic acid) conduits for peripheral nerve regeneration, Biomaterials. 27 (2006) 1035–1042. doi :10.1016/j.biomaterials.2005.07.003. [PubMed: 16098582]

[85]. Rosman B, Barbosa J, Passerotti C, Cendron M, Nguyen H, Evaluation of a novel gel-based ureteral stent with biofilm-resistant characteristics, Int. Urol. Nephrol. 46 (2014) 1053–1058. doi: 10.1007/s11255-013-0636-3. [PubMed: 24366763]

[86]. Cirioni O, Ghiselli R, Silvestri C, Minardi D, Gabrielli E, Orlando F, Rimini M, Brescini L, Muzzonigro G, Guerrieri M, Giacometti A, Effect of the combination of clarithromycin and amikacin on Pseudomonas aeruginosa biofilm in an animal model of ureteral stent infection, J. Antimicrob. Chemother. 66 (2011) 1318–1323. doi:10.1093/jac/dkr107. [PubMed: 21406436]

[87]. Minardi D, Cirioni O, Ghiselli R, Silvestri C, Mocchegiani F, Gabrielli E, d'Anzeo G, Conti A, Orlando F, Rimini M, Brescini L, Guerrieri M, Giacometti A, Muzzonigro G, Efficacy of tigecycline and rifampin alone and in combination against Enterococcus faecalis biofilm infection in a rat model of ureteral stent, J. Surg. Res. 176 (2012) 1–6. doi:10.1016/j.jss. 2011.05.002. [PubMed: 21704328]

[88]. Singh V, Srinivastava A, Kapoor R, Kumar A, Can the complicated forgotten indwelling ureteric stents be lethal?, Int. Urol. Nephrol. 37 (2005) 541–546. doi:10.1007/s11255-004-4704-6. [PubMed: 16307339]

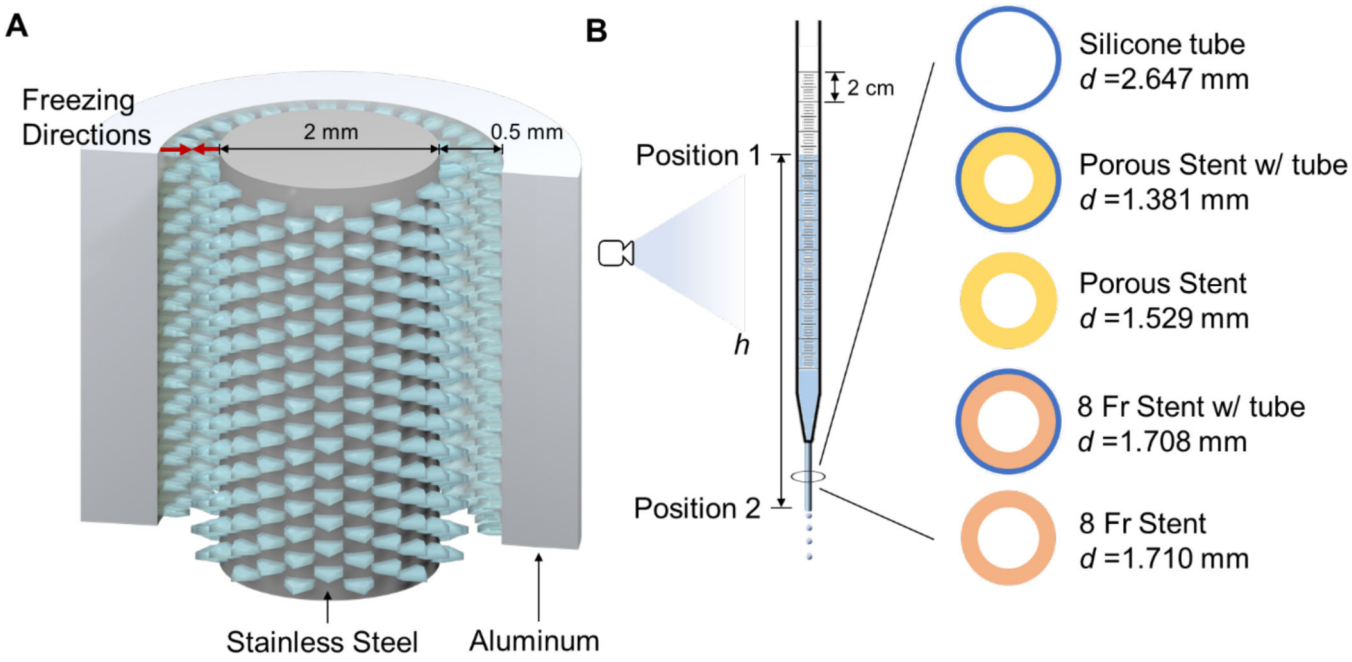

Figure 1.

(A) Tubular mold for the bi-directional freezing of a chitosan slurry, and freezing directions within the mold; (B) schematic of the flow measurement apparatus with schematics of the cross-sections of the five different device configurations tested.

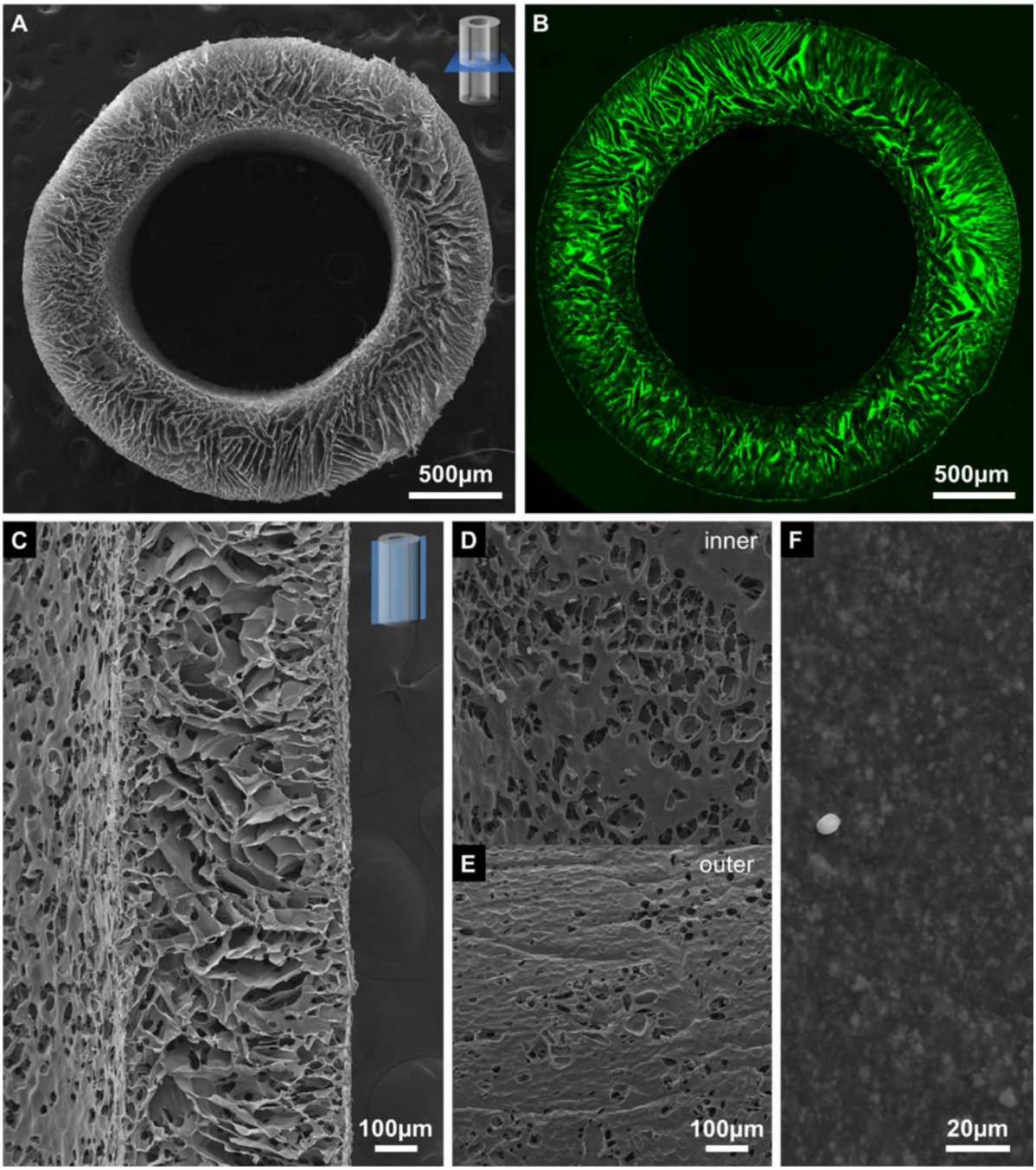

Figure 2.

SEM micrographs of the (A) transverse cross-section, (C) longitudinal cross-section, (D) inner and (E) outer surface of the porous chitosan stent, and inner surface of the 8 Fr stent (F). Confocal micrograph of (B) a transverse cross-section of the porous chitosan stent. The dust particles in (F) was created for imaging purpose. The scale bar on (D) is shared with (E).

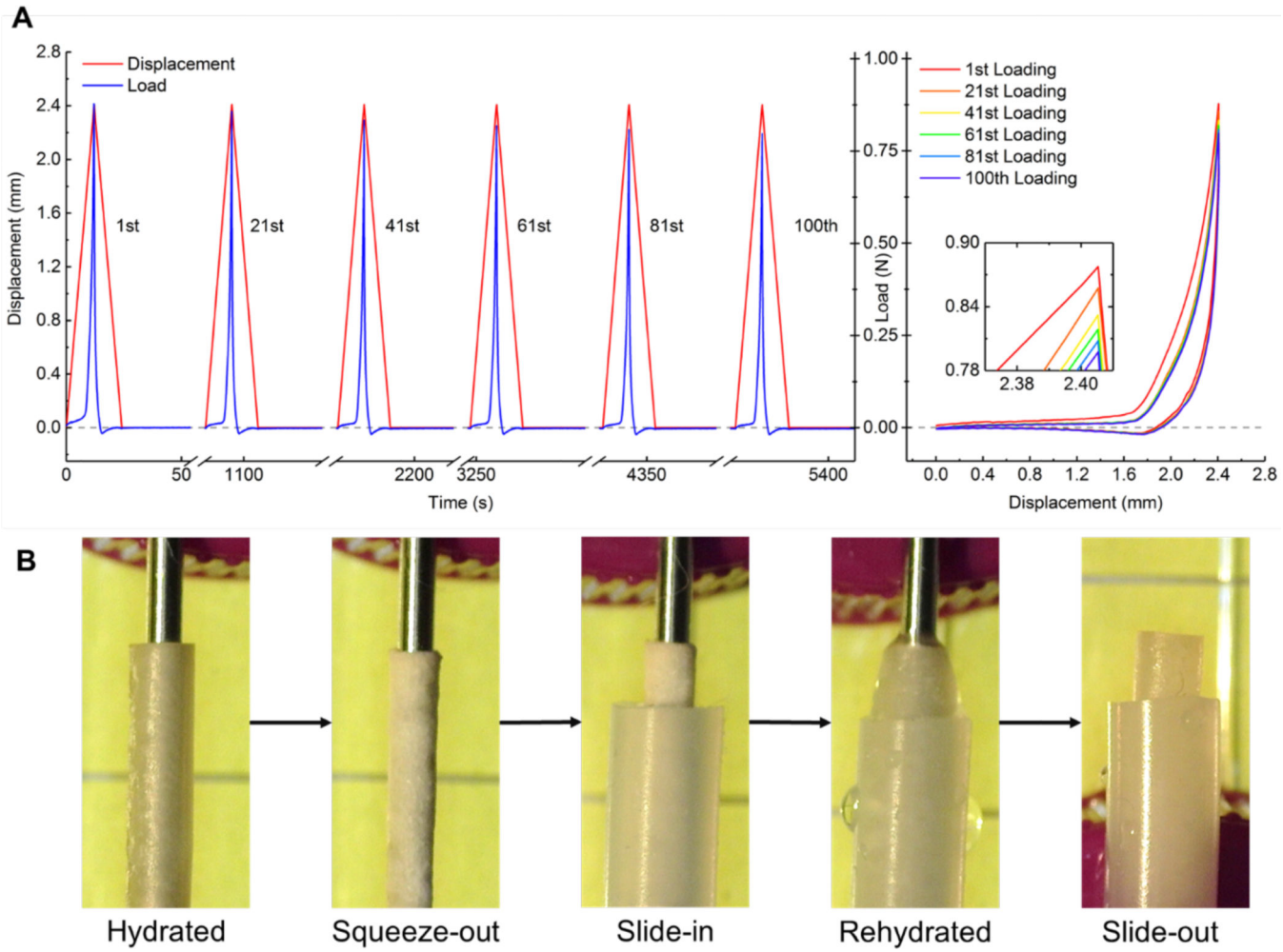

Figure 3.

(A) Displacement and load plotted against time (left) and observed hysteresis (right) during radial compression of the porous chitosan stent. (B) Illustration of the placement and self-expansion and robust positioning of the porous chitosan stent in the silicone tube.

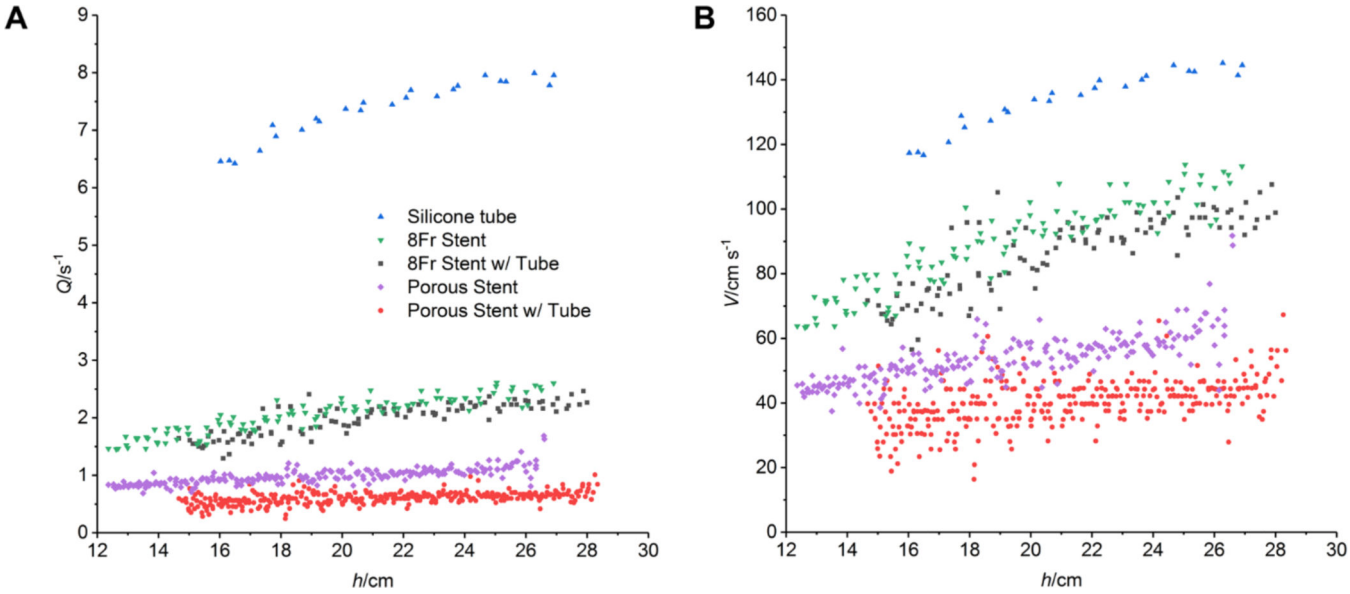

Figure 4.

Volumetric flow (A) and flux (B) in the 8 Fr stents, porous chitosan stents with and without silicone tubes, and silicone tubes at different heights.

Table 1

Diameter of the lumen d, effective viscosity μ_{eff}, and maximum Reynolds number Re_{max} of flow for different designs.

Designs	8 Fr Stent with Tube	8 Fr Stent	Porous Stent with Tube	Porous Stent	Silicone Tube
d/mm	1.708	1.71	1.381	1.529	2.647
Re_{max}	1838	1946	929	1403	3845
μ_{eff}/cP	3.796	2.636	9.267	4.861	*trans.*